

1 Performance of a passive acoustic 2 linear array in a tidal channel

3 Matthew F. Auvinen, David R. Barclay

4 **Abstract**

5 Baseline ambient sound level assessment is important in quantifying anthropogenic noise contributions. Static
6 acoustic sensing in high-flow conditions is complicated by pseudo-sound, or flow noise, caused by turbulent flow
7 on the surface of a hydrophone. Signal processing methods are used to identify and suppress flow noise at low
8 frequencies (< 500 Hz) in data collected on a four-element horizontal hydrophone array in Minas Passage, a tidal
9 channel in the Bay of Fundy, in October 2016. Spectral slope analysis is used to identify the frequencies at which
10 the flow noise and ambient noise contributions to the recorded signal are equal. The maximum frequencies at
11 which flow noise is observed is determined using analysis of the spatial coherence. The array's performance in the
12 Minas Passage is quantified by an empirical relationship between flow speed and the spectral critical frequencies
13 of the coherent output from the linear array. Coherent averaging (broadside beamforming) is demonstrated as an
14 effective flow noise suppression technique, improving low-frequency passive acoustic monitoring in a high-energy
15 tidal channel.

16 **Index Terms**

17 Flow noise, ambient noise, array processing, tidal channel, and passive acoustic monitoring.

18 **I. INTRODUCTION**

19 **T**IDAL power utilities are currently leasing seafloor space within the Minas Passage in the Bay of
20 Fundy with aspirations of converting the energy of the region's tidal currents into electricity, a
21 trend that has been supported by favorable projections of the Passage's tidal energy capacity [1]. It is
22 important that these companies follow sustainable industry practices as the sector grows. This includes the

Dr. David Barclay is an assistant professor in the Department of Oceanography, Dalhousie University. Matthew Auvinen holds a B.Sc. (Hons) from the Department of Oceanography, Dalhousie University, Halifax, NS (email: matthewauvinen@gmail.com; dbarclay@dal.ca).

Manuscript received June 26, 2017; revised MONTTH XX, 201X. This work was supported by the Natural Sciences and Engineering Research Council of Canada, GeoSpectrum Technologies, and Black Rock Tidal Power.

23 consideration of industry knowledge gaps, many of which are a consequence of the sector's immaturity [2].
24 The uncertainty surrounding the ecological and environmental implications of tidal turbine infrastructure
25 is a particularly important knowledge gap and has qualified some opposition to turbine projects.

26 Tidal turbines present two environmental concerns: physical contact (or interaction) with marine life
27 [3] [4] and acoustic pollution. Tidal turbines could become an important source of ambient noise in
28 tidal channels through cavitation and motor or mechanical noise [5]. Turbine anthropophony could affect
29 animal navigation, communication, predator-prey detections [6], and marine life cycles [7]. Moreover,
30 turbine-generated sound could be damaging to fish tissue [8]. If substantive, these effects would threaten
31 near-field and far-field ecosystem health, stressing the need for rigorous environmental impact assessments
32 in the tidal power sector.

33 These environmental risks emphasize the need for baseline ambient noise measurements in the Minas
34 Passage, against which turbine noise pollution will be measured. However, the utility of ambient sensing
35 is limited by pseudo-sound, or flow noise, generated on the surface of a hydrophone in turbulent water.
36 Indeed, the masking effects of flow noise can complicate source identification and background noise
37 assessment in high-flow settings, such as tidal channels.

38 Analogous to turbulent flowing air [9], flowing water in a high Reynolds number regime generates
39 pressure fluctuations on the surface of a hydrophone. These pressure fluctuations produce flow noise
40 which is irregular, uncorrelated, and random. Local pressure fluctuations on the surface of a hydrophone
41 represent near-field turbulence [10]. Free-drifting hydrophones moving with the mean water flow will
42 experience little signal contamination, as it is the relative flow of water over a hydrophone's surface that
43 leads to flow noise.

44 Turbulent flows occupy a wide range of frequencies and wavenumber domains, with broad spatial and
45 temporal variability. The advective nonlinearity of turbulent flows makes them unpredictable in space
46 and time, and contributes to their complex nature [11]. As such, it is difficult to reliably model flow
47 noise. Flow noise follows a spectral slope of $f^{-5/3}$ at low frequencies, behaviour that is analogous by
48 Kolmogorov's turbulence theory. This flow noise is not to be confused with wind-generated noise that
49 produces $f^{-5/3}$ spectral slopes at higher frequencies [12]. Bassett et al. [13] identifies $f^{-5/3}$ flow noise
50 below 20 Hz and also describes steepened spectral slopes, f^{-m} , between 20 and 200 Hz. Lombardi [6]
51 identifies these steep spectral slopes in measurements from the Grand Passage tidal channel. The flow
52 noise that produces f^{-m} is a result of small-scale turbulence being averaged out across the surface of the

53 hydrophones, which dampens (or reduces) measurements.

54 Flow noise presents a unique challenge for passive acoustic monitoring (PAM): a hydrophone in a
55 high-flow setting will record both propagating sound and pseudo-sound. This suggests that models should
56 distinguish between the two sound sources. Barclay and Buckingham [14] describe the exploitation of
57 ambient noise coherence and cross-correlation to address flow noise in deep sea signals. We adapt this
58 application of coherence to identify and suppress flow noise across a four-element array in a tidal channel.

59 Successful suppression of flow noise could benefit PAM systems in relatively energetic environments.

60 The objectives of the present research are:

61 1) Use spectral analysis and spatial coherence to identify and characterize flow noise at low frequencies
62 (< 500 Hz).

63 2) Use coherent averaging (beamforming) to improve the performance of a linear hydrophone array
64 by suppressing flow noise and enhancing the measurement of ambient noise.

65 This paper is organized as follows. Section II discusses important field work details, including an
66 experiment description and instrumentation summary. Section III describes all relevant signal processing,
67 with emphasis on spectral analysis, spatial coherence, and beamforming. Section IV presents the signal
68 processing and data analysis results. Section V evaluates the results and identifies areas for future work.

69 Lastly, Section VI summarizes the findings of the study in a series of conclusions.

70 II. FIELD WORK

71 Field work was completed on October 27, 2016, near the Fundy Ocean Research Center for Energy
72 (FORCE) site in the Minas Passage of the Bay of Fundy. The FORCE site depth ranges between 40 and
73 60 meters depending on the tide. The deployment period spanned roughly four hours, from 12:00 ADT
74 to 16:00 ADT. This experimental window captured the transition from ebb tide to slack tide. Wind speed
75 was measured intermittently throughout the deployment period using a hand-held wind speed gauge. Tidal
76 and flow data was generated using a WebTide model [15].

77 There is a substantial fish population in the Minas Passage [3], some of which could contribute
78 to the local ambient sound field [16]. Pilot whales, dolphins, seals, and other marine mammals that
79 frequent the Minas Passage are another potential source of ambient noise. These animals generate sound
80 through a variety of mechanisms, such as muscle action, stridulation, and vocalization [17]. Non-biological
81 sound sources in the Minas Passage include wave action, anthropogenic activity, and bubbles. Proper

82 characterization of the local sound field at the FORCE site would require consideration these potential
83 sound sources. However, their variability makes source identification challenging.

84 *A. Experiment*

85 A linear hydrophone array was streamed behind the *MV Nova Endeavour* (42' x 16'), which was
86 anchored to the seafloor of the Minas Passage while in dead ship. The array was positioned roughly 15
87 meters below the sea surface using a towfish depressor. The strength of the current kept the array at a
88 relatively constant depth. Four hydrophones were simultaneously sampled over a four hour period and
89 processed by an analog-to-digital converter (ADC) on board the *MV Nova Endeavour*. The signal cable,
90 which carried both the array and a drogue, was sheathed in a fairing to reduce strum generation and
91 attached to a tow cable (6GA galvanized wire) using cable ties.

92 A drifting hydrophone (Geospectrum Technologies GuardBuoy) was deployed using a small auxiliary
93 vessel launched from the *MV Nova Endeavour*. The GuardBuoy was suspended 2 meters below the surface
94 using a drifting surface float and isolation system made of a damping mass and a Dacron non-stretch line
95 and compliant bungee. The system isolated the recording hydrophone and instrument package from any
96 surface action, such as the vertical movement of waves, which would otherwise generate mechanical or
97 flow noise.

98 A total of five transects were performed by driving the GuardBuoy upstream in a rigid-hulled inflatable
99 boat (RHIB), deploying the drifter, turning off the RHIB engines, and then floating downstream with at
100 least 15 meters between the RHIB and the GuardBuoy. The GuardBuoy and RHIB followed a downstream
101 transect that passed over the array. The GuardBuoy was retrieved once it had reached 20 meters beyond
102 the array. These transects were performed over the course of three hours, beginning at 13:00 ADT. The
103 GuardBuoy signals are assumed to be free of flow noise and were used as benchmarks to assess the
104 performance of the array. The turbulent tidal channel is assumed to be well mixed with an isovelocity
105 sound speed profile, minimizing noise field variability over the depth difference between the two systems.

106 *B. Instrumentation*

107 The linear array is an oil-filled array with a rigid exterior and acoustically transparent outer skin.
108 It contains four sequentially spaced hydrophones with a horizontal configuration along the axis of the
109 array. The array and the hydrophones were constructed by GeoSpectrum Technologies. Each neighbouring
110 hydrophone is separated by a distance $d = 17\text{cm}$. The array hydrophones were set to simultaneously sample

111 at a rate of 96 kHz with an acoustic bandwidth of 48.019 kHz. The four channels on the array continuously
 112 recorded 10 minute WAV files over a 4 hour period. Power spectra were calibrated to dB re 1 μ Pa according
 113 to frequency-dependent sensitivities supplied by the manufacturer. The GuardBuoy sampled at a rate of
 114 96 kHz with an acoustic bandwidth of 48 kHz, and was equipped with a GPS to record transect geospatial
 115 information. The Guard Buoy recorded WAV files in 30 minute segments. Corresponding power spectra
 116 were converted to dB re 1 μ Pa according to frequency-dependent sensitivities supplied by the manufacturer.

117 III. DATA ANALYSIS

118 Data analysis was performed in MATLAB in several stages. The analysis began with the calculation of
 119 the power spectral density (PSD) from the raw WAV files, followed by spectral analysis, spatial coherence
 120 analysis, and broadside beamforming.

121 *A. General Signal Processing*

The output of a hydrophone is defined as

$$x_i(t) = \sigma_i(t) + n_i(t) \quad (1)$$

122 where x_i is the recorded time series on each i th hydrophone, σ_i is the sound field's ambient components,
 123 and n_i is the locally generated flow noise. Importantly, n_i and σ_i are uncorrelated. Furthermore, the
 124 inherent randomness of flow noise makes n_i incoherent with respect to n_j .

125 The power spectrum, or spectral density, is defined as

$$S_{ii}(\omega) = \frac{\langle X_i(\omega) \cdot X_i^*(\omega) \rangle}{T} \quad (2)$$

126 where X_i is the Fourier transform of x_i , ω is angular frequency, $*$ denotes a complex conjugate, $\langle \rangle$
 127 indicates an ensemble average, and T is the observation interval. All Fourier transforms are windowed
 128 by a Hann function. The Hann function's effect on the variance has been accounted for. The time series
 129 were divided into 34.1 second-long segments, where each segment was further split into 50 contiguous
 130 subsegments of 0.682s with no overlap. A 2^{16} Fourier transform was applied to each subsegment, from
 131 which ensemble averaging produced a power spectral density with a frequency bin width of 1.47 Hz.
 132 Coherence is used to quantify the similarity between two signals and is defined as

$$\Gamma_{ij}(\omega) = \frac{S_{ij}(\omega)}{(S_{ii}(\omega) \cdot S_{jj}(\omega))^{\frac{1}{2}}}. \quad (3)$$

133 **B. Power Spectrum Probability Density**

134 Spectral probability density (SPD) is an analytical technique used to depict the variability of the power
 135 spectrum over a period that is much longer than the minimum time required for a stationary measurement
 136 of power to be made [18]. This form of analysis facilitates the identification of unique events within a
 137 series of spectra. The power spectrum probability density (PSPD) is defined as

$$\text{PSPD}(f) = H(S_{ii}(f), h) \quad (4)$$

138 where $\text{PSPD}(f)$ is the power spectrum probability density at frequency f , and $H(S(f), h)$ is the histogram
 139 of the power spectrum S_{ii} at frequency f with a histogram bin width of h dB re $1 \mu\text{Pa}^2/\text{Hz}$. By combining
 140 PSPD results across frequencies, we generate a PSPD matrix

$$\begin{bmatrix} \text{PSPD}(f_1) & \text{PSPD}(f_2) & \text{PSPD}(f_3) & \dots & \text{PSPD}(f_a) \end{bmatrix} \quad (5)$$

141 where $\text{PSPD}(f_a)$ is the PSPD at the a th frequency.

142 **C. Spectral Critical Frequency**

143 Lombardi [6] and Bassett et al. [13] suggest that there are three distinct spectral slope regions in
 144 the low-to-mid-frequency range: spectral slopes of Kolmogorov's $f^{-5/3}$; steepened flow noise spectral
 145 slopes, f^{-m} , that include the effects of a finite volume sensor [13]; and an ambient noise region that is
 146 determined by near-field and far-field ambient sound sources.

The local spectral slope is defined as

$$-M = \frac{S_{ii}(2\pi f_a) - S_{ii}(2\pi f_b)}{\log(f_a \cdot f_b^{-1})} \quad (6)$$

147 where $S_{ii}(2\pi f_a)$ is the spectral density on the i th sensor at frequency f_a and $S_{ii}(2\pi f_b)$ is the spectral
 148 density on the i th sensor at frequency f_b . (6) describes the spectral slope in dB/decade.

149 The transition from the flow noise region of f^{-m} to the ambient noise region is marked by the frequency
 150 knee, where the spectral slope begins to shallow. That is, the exit from the flow noise region is marked by

151 a deviation below the slope f^{-m} . Here, the spectral critical frequency, f_c , is defined as the first frequency
 152 at which

$$|M| < |m| \quad (7)$$

153 is true. Importantly, both slopes in (7) are in dB/decade.

154 *D. Coherence Critical Frequency*

155 Spatial coherence is calculated for each channel combination using (3), providing an assessment of
 156 signal similarity between elements. Propagating ambient noise is highly correlated across the array.
 157 Additionally, propagating noise at wavelengths sufficiently large relative to element spacing produces
 158 very high coherence at low frequencies by effectively co-locating sensors. Conversely, flow noise is a
 159 source of incoherence, as pseudo-sound is uncorrelated across the linear array (when turbulent scales are
 160 lesser than hydrophone separation). Therefore, in the band $f < 500$ Hz, flow noise is marked by low
 161 coherence while ambient noise is marked by high coherence. The transit of this coherence boundary, from
 162 flow noise (incoherent) to ambient noise (coherent) provides a metric for describing the extent of flow
 163 noise across the array.

164 The coherence critical frequency, f'_c , is defined as the frequency at which a minimum coherence
 165 threshold is crossed due to flow noise masking. To establish this coherence threshold, we assume an
 166 isotropic ambient noise field such that the horizontal coherence is given by Buckingham [19]

$$G_{ij}(\omega') = \frac{\sin(\omega'_{ij})}{\omega'_{ij}} \quad (8)$$

167 where

$$\omega'_{ij} = \frac{2\pi d_{ij} f}{c}. \quad (9)$$

168 Here, d_{ij} is the separation distance between the i th and j th hydrophone and c is the local sound speed.
 169 We define f'_c as the first frequency at which

$$|\Gamma_{ij}(\omega')| \geq 0.9 \cdot G_{ij}(\omega') \quad (10)$$

is true. We can be confident that any coherence within 10% of (8) is real and significant while any drop below the threshold given by the right hand side of (10) is caused by the addition of flow-generated incoherent noise. This automated critical frequency detector corresponds to a coherence threshold of ~ 0.9 . The use of a more sophisticated noise model such as Cron and Sherman [20] or Deane et al. [21] in the place of (8) yields a nearly identical threshold.

175 E. Linear Regression

176 Least squared linear regressions between critical frequencies, f_c and f'_c , and flow speed, u , are used to
 177 identify and characterize the prevalence of flow noise and ambient noise in measurements. No data points
 178 are excluded from these regressions.

179 F. Beamforming

180 We use a broadside beamformer to coherently average the channels across the array. Locally generated
 181 flow noise and the ambient sound field are inseparable, however we can describe their relative prevalence
 182 with the theoretical signal-noise ratio (SNR) where we are defining ambient sound as the signal, and flow
 183 noise as the noise. By taking the Fourier transform of (1) and substituting into (2), we find

$$S_{ii} = \frac{\langle (\varsigma_i + N_i) \cdot (\varsigma_i^* + N_i^*) \rangle}{T} \quad (11)$$

184 where ς_i and N_i are the Fourier transforms of σ_i and n_i , respectively. For clarity, the frequency dependency
 185 has been omitted. Since ς_i and N_i are uncorrelated, we can expand (11) to arrive at

$$S_{ii} = \frac{\langle \varsigma_i \varsigma_i^* \rangle + \langle N_i N_i^* \rangle}{T}. \quad (12)$$

186 Given (12), the SNR for a single hydrophone (SNR_H) is defined as

$$\text{SNR}_H = \frac{\langle \varsigma_i \varsigma_i^* \rangle}{\langle N_i N_i^* \rangle} \quad (13)$$

187 where $\text{SNR}_H = 1$ at the critical frequency, f_c . Now consider an array of hydrophones indexed by i , where
 188 the ambient sound field component of the signal on each phone is

$$\sigma_{i+1}(t) = \sigma_1(t - \tau_i) \quad (i > 1) \quad (14)$$

189 where

$$\tau_i = \frac{i \cdot d \cos \theta}{c} \quad (15)$$

190 is the acoustic travel time in seconds for plane wave noise arriving on the sensors at the angle θ . Here,
 191 d is the nearest neighbour element separation. Taking the Fourier transform of (14) gives

$$\varsigma_i(\omega) = \varsigma_1(\omega) e^{-i\omega\tau_i}. \quad (16)$$

192 The coherent sum of the signals across the array is defined as

$$x_T(t) = \sum_{i=1}^l x_i(t) \quad (17)$$

193 where $x_i(t)$ is the signal recorded on the i th element of a linear array l elements long. Since no time
 194 delay has been applied to $x_i(t)$, $x_T(t)$ is the equivalent to beamforming broadside to the array. Since the
 195 source of interest is ambient noise, the sound field is assumed to be axially symmetric. Thus the horizontal
 196 array orientation and beam direction are unimportant, provided an appropriate array gain compensation
 197 is applied.

198 The Fourier transform of (17) is

$$X_T(\omega) = \sum_{i=1}^l X_i(\omega). \quad (18)$$

¹⁹⁹ The array power spectral density can be estimated using (18) by

$$A = \frac{\langle X_T(\omega) \cdot X_T^*(\omega) \rangle}{T}. \quad (19)$$

²⁰⁰ Given an array with both ambient noise and flow noise components, (18) can be expanded to

$$X_T = [\varsigma_1 + N_1 + \varsigma_2 + N_2 + \dots + \varsigma_l + N_l] \quad (20)$$

²⁰¹ which describes the total output of all sensors on an array with l elements. Substituting (16) into (20)
²⁰² gives

$$X_T = \varsigma_1 + N_1 + \sum_{i=1}^l (\varsigma_i e^{-i\omega\tau_i} + N_{i+1}). \quad (21)$$

²⁰³ Using the Fourier transform of the coherently summed outputs across the array, the power spectral density
²⁰⁴ can be computed by substituting (21) into (19) yielding

$$A = \frac{\langle \varsigma_1 \varsigma_1^* \left[l + \sum_{i=1}^{l-1} \frac{1}{2} (l-i) \cos(\omega\tau_i) \right] + N \cdot N^* \rangle}{T} \quad (22)$$

²⁰⁵ where

$$N = \sum_i^l N_i \quad (23)$$

²⁰⁶ is the coherently summed flow noise. This term can be simplified by assuming the power of the flow
²⁰⁷ noise measured on each individual hydrophone is equal across the array,

$$\langle N_i N_i^* \rangle = \langle N_j N_j^* \rangle \quad (24)$$

²⁰⁸ and uncorrelated between the sensors,

$$\langle N_i N_j^* \rangle = \delta_{ij} \cdot N_1 N_1^* \quad (25)$$

²⁰⁹

$$\delta_{ij} = \begin{cases} 0 & \text{if } i \neq j \\ 1 & \text{if } i = j. \end{cases}$$

²¹⁰ Then the total power received by the array becomes

$$A = \frac{\langle \zeta_1 \zeta_1^* \rangle \left[l + \sum_{i=1}^{l-1} \frac{1}{2} (l-i) \cos(\omega \tau_i) \right] + l \langle N_1 N_1^* \rangle}{T}. \quad (26)$$

²¹¹ Furthermore, if K is defined as

$$K = l + \sum_{i=1}^{l-1} \frac{1}{2} (l-i) \cos(\omega \tau_i) \quad (27)$$

²¹² then (26) becomes

$$A = \frac{K \langle \zeta_1 \zeta_1^* \rangle + l \langle N_1 N_1^* \rangle}{T} \quad (28)$$

²¹³ where (28) describes the array spectral density. Here, SNR_A describes the relative strength of the ambient
²¹⁴ noise and flow noise components of the array output, such that

$$SNR_A = \frac{K \langle \zeta_1 \zeta_1^* \rangle}{l \langle N_1 N_1^* \rangle}. \quad (29)$$

²¹⁵ Comparing (29) to the result derived for a single hydrophone, given by (13), we see that the beamformed
²¹⁶ array improves the signal-to-noise ratio by a factor of $\frac{K}{l}$. Furthermore, (29) suggests that array performance

improves with an increasing number of hydrophones, l . For an array with 4 elements, at broadside, $\frac{K}{l} = \frac{7}{4}$.

219 G. Array Gain

220 The broadside beamforming analysis applied to the linear array generates artificial spectral density gain.
 221 As a result, an array gain formula is applied to the beamformed results to correct the inflated values. The
 222 array gain formula presented here is adapted from Cox [22], such that

$$AG = 10 \log l. \quad (30)$$

223 The array gain correction is performed by subtracting the result of (30) from the calculated array power
 224 spectral density.

225 H. Algorithm Assessment

226 All channel signals are consolidated into one coherent array output using (18) and (19). The resulting
 227 coherent array signal is compared to signals from the GuardBuoy and a single fixed hydrophone to evaluate
 228 the performance of the beamformed array. The algorithm is further tested by comparing the coherent array
 229 spectral critical frequencies to the spectral critical frequencies of a fixed single hydrophone.

IV. RESULTS

231 A. Spectral Density

232 A comparison between spectral density and current speed (Fig. 1) reveals high signal levels in fast
 233 flowing water and low signal levels in slow flowing water. The signal power is high below 10 Hz and falls
 234 off as the frequency approaches 100 Hz, which indicates that flow noise is prevalent at low frequencies.

235 The hydrophone power spectrum contains multiple episodes of mid-frequency noise. These signals are
 236 attributed to ship noise generated by passing ships and the small vessel used in the GuardBuoy drifter
 237 tests. The abrupt shift in spectral density at 90 minutes is attributed to a reset of the ground between the
 238 data acquisition hardware and the array housing. The data collected during the reset have been omitted.

239 *B. Power Spectrum Probability Density*

240 The PSPD (Fig. 2) facilitates the broad-scale assessment of a hydrophone's spectral density over entire
241 deployment periods. The PSPD follows a spectral slope of $f^{-5/3}$ below 10 Hz, behaviour analogous to
242 Kolmogorov's turbulence theory. This spectral slope marks a region of flow noise within the signal. A
243 steepened spectral slope of f^{-m} , where $m > \frac{5}{3}$, persists between 40 and 100 Hz, a result of small-scale
244 turbulence when turbulence wavelength \ll sensor size. This small-scale turbulence is averaged out over
245 the surface of the hydrophone sensor, dampening the measured signals. The PSPD results show that
246 ambient noise is dominant above 300 Hz, where signal levels are markedly low. Single power spectra are
247 superimposed on the PSPD and suggest that measurements in slow current conditions contain a greater
248 extent of ambient noise relative to those in fast current conditions.

249 Early in the deployment (around 10 minutes) electronic noise in the system raised the noise floor to 90
250 dB μ Pa. While this was quickly remedied on site and has been accounted for in the data, a noise floor
251 persisted around 60 dB μ Pa.

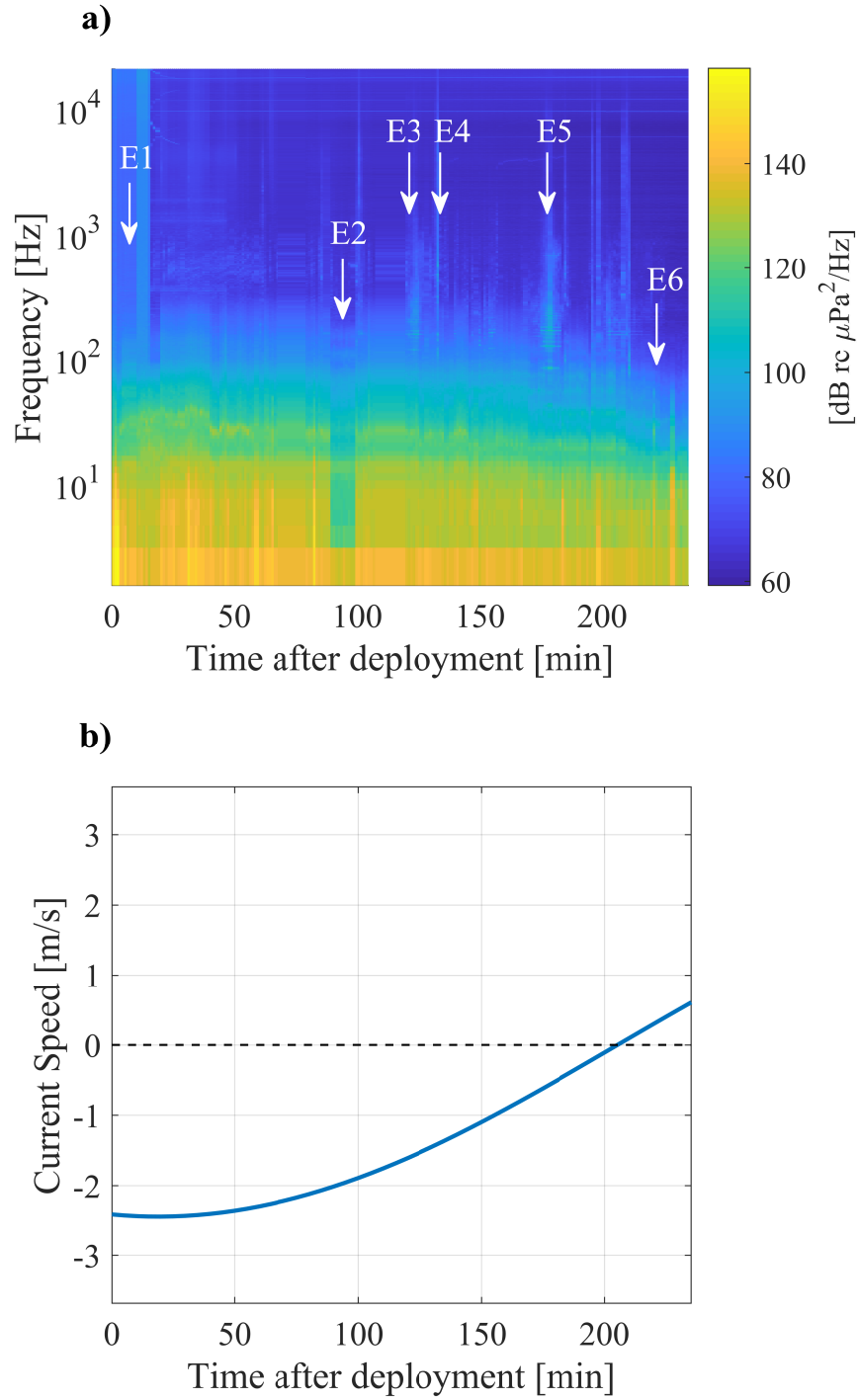


Fig. 1. Power spectrum for channel 0 on the array (a). The spectrum is plotted over the deployment period across a range of low-to-mid frequencies. Different mid-frequency noise events are represented by E1 - E6. The spectrum begins at maximum ebb tide and ends shortly after slack tide, as shown by the current speed time series (b). Power decreases with current speed over the deployment period.

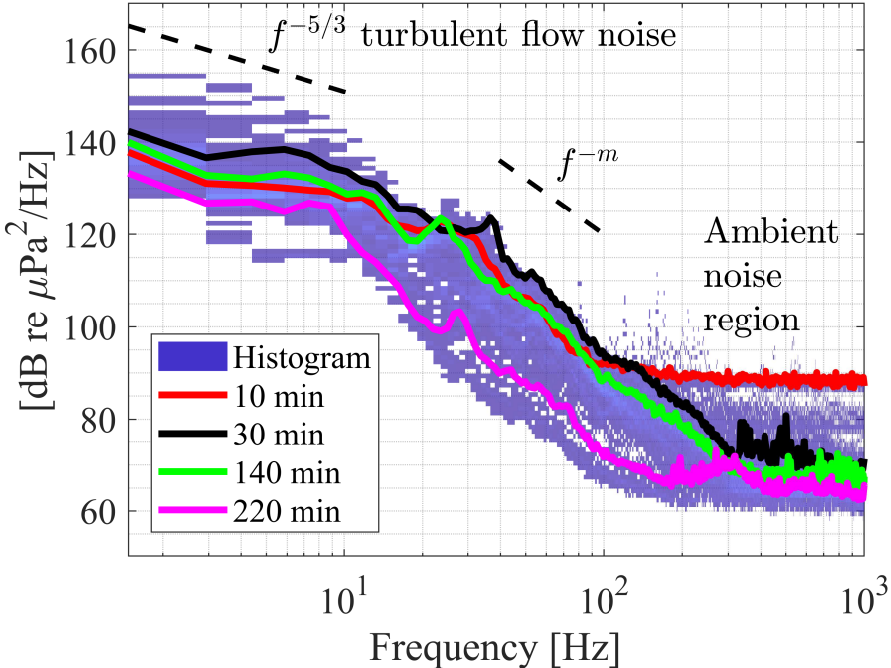


Fig. 2. Fixed single hydrophone power spectrum probability density over the entire deployment period. Turbulent flow noise is prevalent $< 10 \text{ Hz}$ (where wavelengths $>>$ sensor size), with a spectral slope of $f^{-5/3}$, while turbulence interacting with the hydrophone's finite volume (in the 10 Hz to 100 Hz band) yields a spectral slope of f^{-m} . The ambient sound field dominates at frequencies $> 300 \text{ Hz}$. Coloured lines represent individual spectra recorded at the time after deployment indicated in the legend.

252 C. Spectral Critical Frequency

253 Spectral slopes were calculated between 40 and 100 Hz for each minute of deployment using (6). The
 254 linear relationship between spectral slope, m , and current speed, u , (Fig. 3) indicates that signals recorded
 255 in decreasing flow are increasingly damped (steepened slope). The inverse relationship between current
 256 speed and spectral slope suggests that signals are less damped in fast flowing water, a result of larger
 257 turbulence scales. The spectral slopes observed between 40 and 100 Hz range from -25 to -60 dB/decade.
 258 The correlation coefficient, R , indicates that there is a meaningful correlation between spectral slope and
 259 current.

260 The spectral critical frequency was calculated for each minute of deployment using (7). These critical
 261 frequencies were regressed against current speed, as shown in Fig. 4. There is a positive correlation
 262 between spectral critical frequency and current speed, where fast flow coincides with high spectral critical
 263 frequencies. The spectral critical frequency is the frequency at which flow noise and ambient noise are
 264 equal in power.

265 The intercepts have not been forced to zero. This is because it is unrealistic to expect that we can com-
 266 pletely eliminate flow noise, or low-frequency noise generated by the mechanical systems that comprise

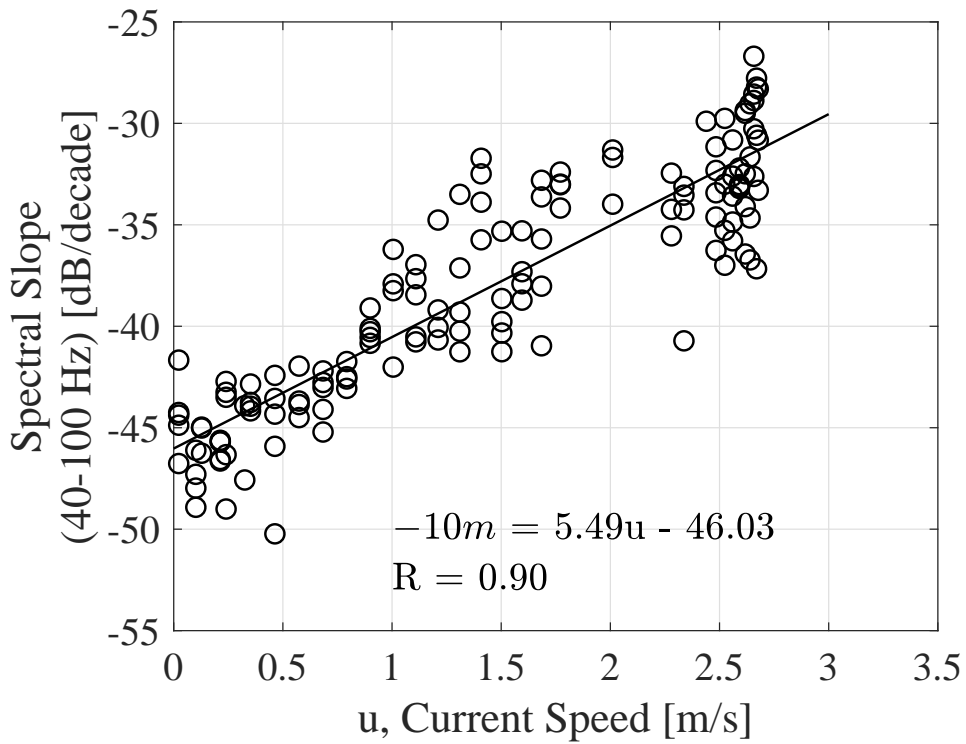


Fig. 3. Relationship between spectral slope, m , and current speed, u , between 40 and 100 Hz for channel 0. Spectral slope magnitude increases with decreasing flow. The correlation coefficient, R , is reported.

267 the tow body. If this were a moored system with no surface expression, that assumption might be valid,
268 but is not considered here.

269 *D. Spatial Coherence*

270 Spatial coherence is calculated for different hydrophone combinations across the linear array using (3).
271 The spatial coherence results are presented in magnitude coherence for the entire deployment period (Fig.
272 5).

273 If the wavelength of propagating sound is sufficiently long (frequency sufficiently low) the sensors would
274 become relatively co-located and the coherence would tend to unity. However, the results suggest that
275 the low frequency data is overwhelmingly incoherent, since the locally generated flow noise is incoherent
276 from one hydrophone to the next.

277 Flow noise is uncorrelated and propagating ambient noise is highly correlated at low frequencies. As
278 a result, low coherence and high coherence are a sign of flow noise and ambient noise, respectively.
279 Therefore, the spatial coherence results are partitioned into two distinct regions: a flow noise region
280 and an ambient noise region. Visual assessment suggests that flow noise is consistently present at low

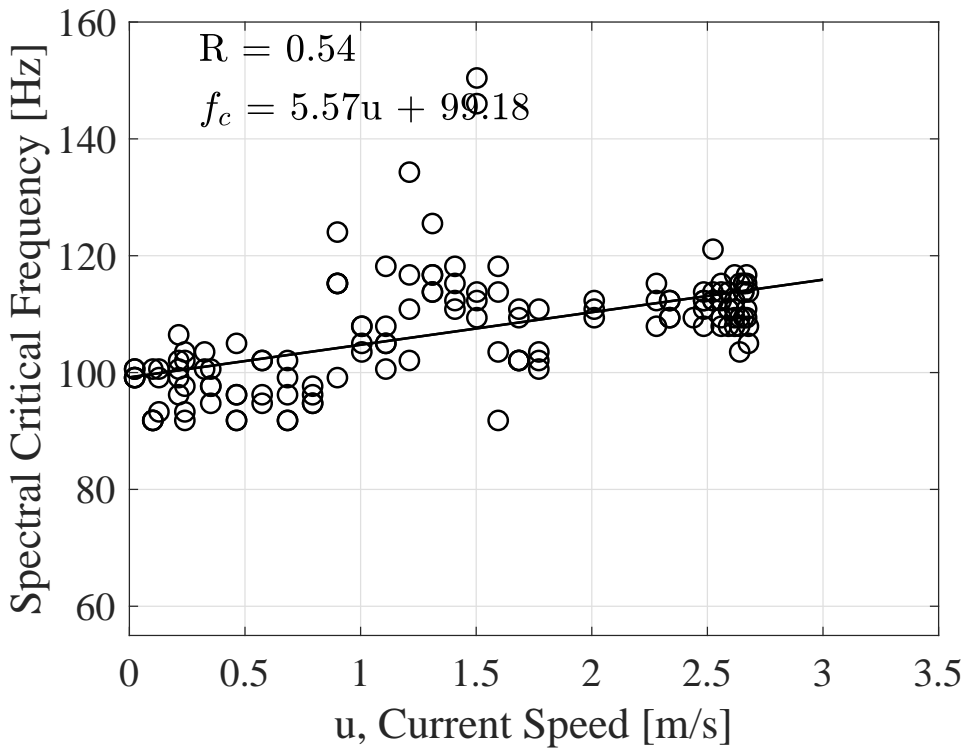


Fig. 4. Relationship between spectral critical frequency, f_c , and current speed, u , for channel 0. Spectral critical frequency marks where the flow noise and ambient noise contributions to the recorded signal are equal, and increases with current speed. Correlation coefficients, R , are reported.

281 frequencies and can be prominent at higher frequencies (above 600 Hz). The ambient noise region is
 282 present between 200 and 600 Hz and contains the same vessel noise identified in Fig. 2.

283 *E. Coherence Critical Frequency*

284 The coherence critical frequency is the highest frequency at which flow noise can be detected. The
 285 coherence critical frequency was calculated for each minute of deployment for each combination of chan-
 286 nels, and is used to quantify the relative prevalence of flow noise and ambient noise within a measurement
 287 (Fig. 6). The coherence critical frequency is a more sensitive method of flow noise measurement than
 288 the spectral critical frequency, as spatial coherence is used as an indicator of flow noise cessation rather
 289 than relative noise contributions. The coherence critical frequency increases with increasing flow speed,
 290 a relationship similar to that of the spectral critical frequency.

291 It is important to note that the coherence is impacted by any temporary deterministic noises present in
 292 the sound field, such as the auxiliary RHIB, mechanical array noise, or noise generated aboard the *MV*
 293 *Nova Endeavour*. In such instances, the automated coherence critical frequency detector fails, and yields
 294 an outlier. These outliers have been removed.

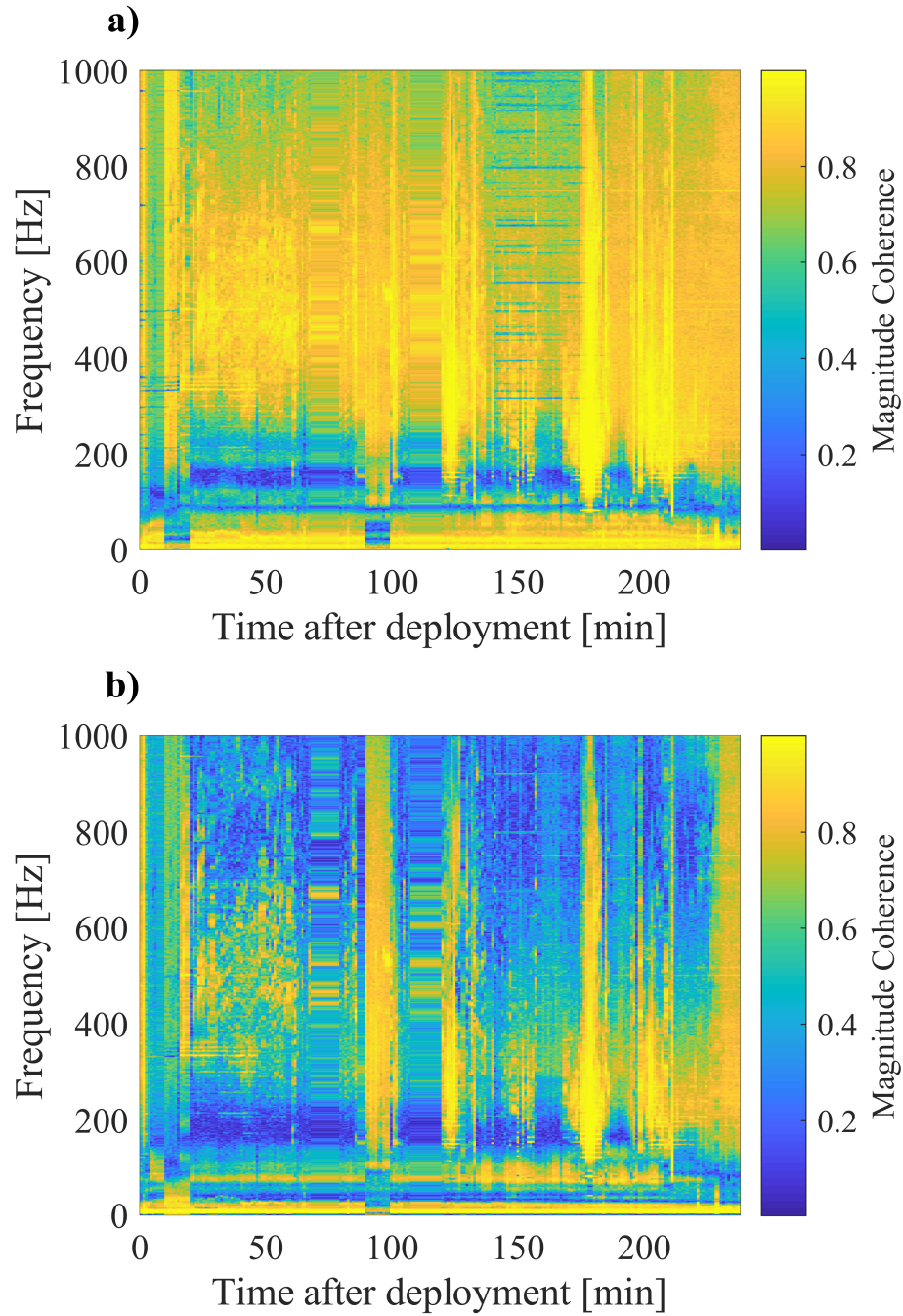


Fig. 5. Spatial coherence over the experimental period. Magnitude coherence is expected to tend to unity as the fixed hydrophones become relatively co-located. However, uncorrelated flow noise on each phone breaks that relationship. The extent of incoherent flow noise increases with current speed. Channel 0 - 1 (a) and 0 - 3 (b) are shown as examples. Results hold to all other channel combinations.

295 *F. Beamforming*

296 The spectral critical frequency of the coherent array output is compared to the fixed single hydrophone
 297 spectral and coherence critical frequencies in Fig. 7. The standard deviations of the spectral slope and

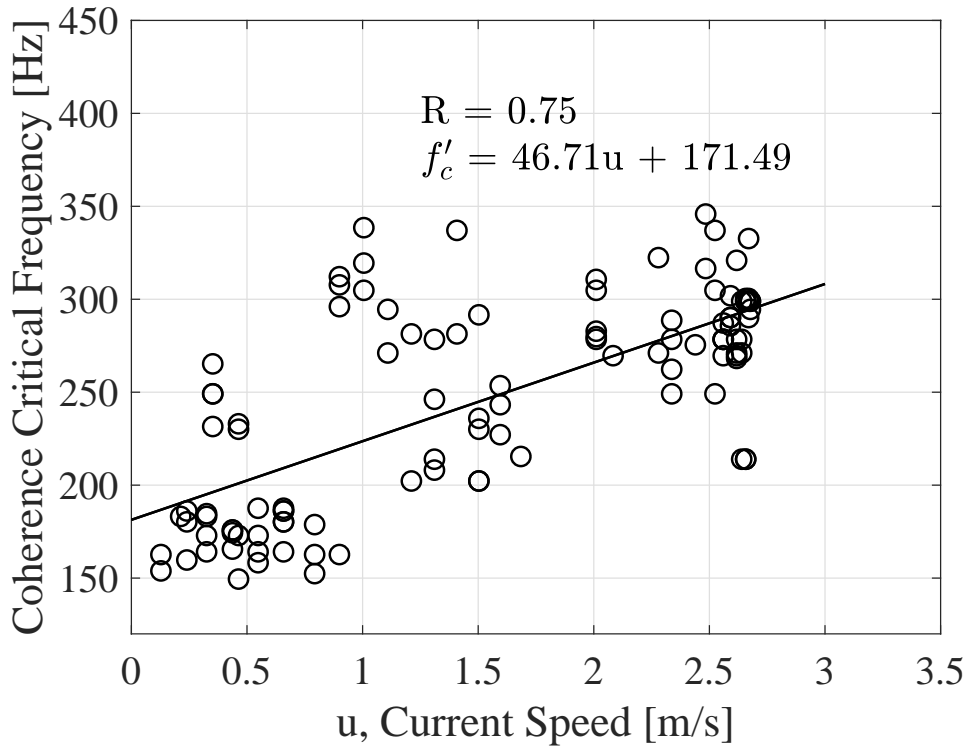


Fig. 6. Relationship between coherence critical frequency, f'_c , and current speed, u , for channels 0 - 1. Coherence critical frequency is the highest frequency at which flow noise can be detected, and increases with current speed.

298 spatial coherence critical frequency regressions were extracted from the averaged fits, while the standard
299 deviation of the coherent array critical frequency regression was calculated from the data during the
300 regression.

301 The coherence critical frequencies are relatively high, while spectral critical frequencies (both fixed
302 single hydrophone and coherent array) are relatively low. This is attributed to the more sensitive nature
303 of the coherence-based method. Above coherence critical frequencies we can be confident that there is
304 no contamination of the ambient noise field by flow noise. Conversely, the fixed single hydrophone and
305 coherent array spectral critical frequencies show where flow noise and ambient noise have equal power.
306 The coherence and spectral critical frequencies serve as the respective upper and lower bounds of different
307 noise regimes. Importantly, the coherent array output contains lower critical frequencies than the fixed
308 single hydrophone, indicating that the broadside beamforming approach lessens the extent of flow noise
309 within the measurements.

310 Fig. 8 compares GuardBuoy, fixed single hydrophone, and horizontal coherent array power spectra at
311 1.5 hours into the experiment. We select a time where the drifter and array were in close proximity to
312 establish a meaningful comparison.

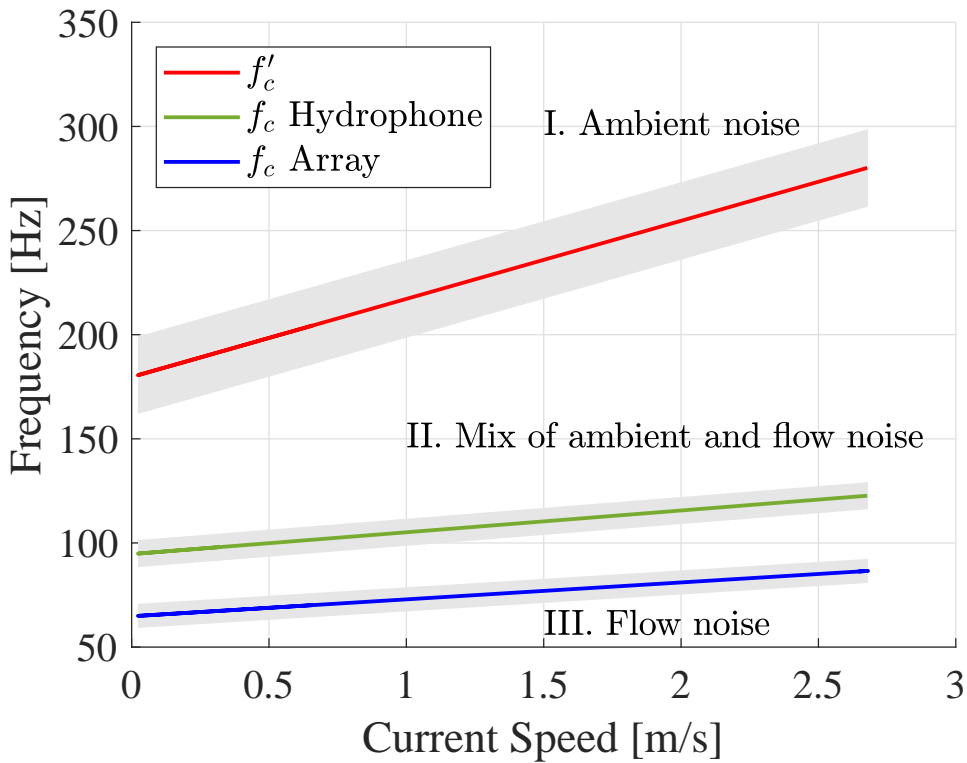


Fig. 7. Comparison of fixed single hydrophone spectral critical frequency (green), array spectral critical frequency (blue), and coherence critical frequency (red) as a function of current speed. Uncertainties are one standard deviation (shaded). Coherence critical frequency, f'_c , separates region I, where flow noise is negligible, and region II, where flow and ambient noise are both present, while spectral critical frequency, f_c , separates regions II and III, where flow noise dominates. The coherent array effectively suppresses flow noise, as indicated by its lower boundary relative to the fixed single hydrophone.

313 The GuardBuoy spectrum behaves differently from the rest, exhibiting lower levels at frequencies
 314 below 100 Hz. A pronounced excursion in spectral slope is present at 10 Hz in the GuardBuoy spectrum,
 315 suggesting non-negligible flow noise is affecting the drifter's low-frequency measurements. This is typical
 316 of all moored or free drifting passive acoustic systems that have a surface expression or subsurface float.
 317 The fixed single hydrophone shows clear symptoms of flow noise at low frequencies.

318 The spectra reveal that the coherent array spectra transitions to the ambient noise region at lower
 319 frequencies than the fixed single hydrophone. Furthermore, the coherent array signals are quieter than
 320 the fixed single hydrophone signals at all low frequencies, demonstrating the effective suppression of
 321 flow noise. There is reasonable agreement between the GuardBuoy and coherent array above the critical
 322 frequency, with some difference above 700 Hz. This disparity is attributed to the lack of co-location
 323 between the array and the GuardBuoy, as they are vertically and horizontally displaced relative to each
 324 other.

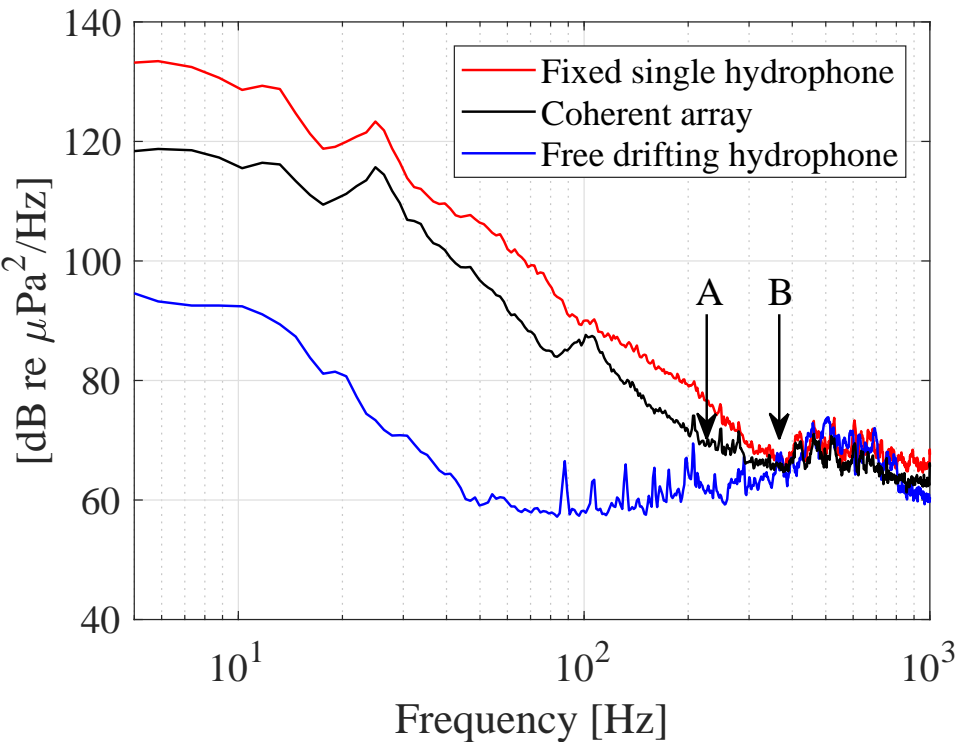


Fig. 8. Comparison of fixed single hydrophone (red), coherent array (black), and free drifting hydrophone (blue) signal power spectra at 1.5 hr into the deployment. The current speed at this moment was 2.2 m/s. A and B indicate the spectral critical frequencies of the coherent array and the fixed single hydrophone, respectively. The reduced levels and spectral critical frequency of the coherent array output relative to the fixed single hydrophone indicates effective flow noise suppression.

325

V. DISCUSSION

326 A. Spectral Critical Frequency

327 Results show that critical frequency and flow speed are positively related, giving the intuitive result
 328 that flow noise is prevalent in fast current conditions. The spectral critical frequency presents a method
 329 of identifying flow noise prevalence within a signal.

330 The spectral critical frequency marks where ambient noise and flow noise have equal power, and
 331 provides two important insights. Firstly, frequencies above the spectral critical frequency will contain a
 332 mixture of ambient noise and flow noise. Secondly, frequencies below the spectral critical frequency will
 333 be dominated by flow noise, since measurements in these frequencies contain spectral slopes that align
 334 with turbulence theory. These insights are important, as they provide useful context for future signal level
 335 and sound-source evaluations in tidal channel measurements.

336 *B. Spatial Coherence*

337 Spatial coherence results for different sensor combinations show that there are two distinct coherence
 338 regions across the array: an incoherent flow noise region and a coherent ambient noise region. The
 339 prevalence of these regions is quantified with the coherence critical frequency. Iterative calculations of the
 340 coherence critical frequency were regressed against current speed. There is a positive relationship between
 341 coherence critical frequency and current speed. The coherence critical frequency marks the frequency above
 342 which flow noise is absent.

343 The spectral critical frequency provides a lower boundary, below which ambient noise is negligible,
 344 and the coherence critical frequency provides an upper boundary, above which flow noise is negligible.
 345 Frequencies between these bounds contain a mixture of flow noise and ambient noise. This explains why
 346 the coherence critical frequencies are noticeably higher than those of the spectral method. The application
 347 of spectral and coherence critical frequencies provides insight on the relative extent of both ambient noise
 348 and flow noise within a signal.

349 *C. Beamforming*

350 By effectively treating the array as one sensor or hydrophone, signal processing can address the pseudo-
 351 sound within low frequency data. Coherent averaging suppresses flow noise and enhances the detection of
 352 propagating ambient noise. The coherent averaging employs a broadside approach with no steering angle
 353 (19).

354 The results of the spectral critical frequencies derived from the beamformed array are shown in
 355 Fig. 7. Evidently, the coherent array contains lower levels and lower critical frequencies than the fixed
 356 single hydrophone (Fig. 7; Fig. 8). This implies that the coherent array is less affected by flow noise, and
 357 contains a greater extent of ambient noise.

358 VI. CONCLUSION

359 Flow noise appears as: $f^{-5/3}$ noise when wavelength \gg sensor size, and f^{-m} noise, where the sensor's
 360 finite dimension reduces the flow noise. f^{-m} is related to the flow speed over the array. The spectral critical
 361 frequency is used to identify where ambient noise is negligible and the coherence critical frequency is
 362 used to identify where flow noise is negligible.

363 Coherent processing (beamforming) suppresses flow noise and yields a lower spectral critical frequency
 364 than that of a fixed single hydrophone. An increased number of hydrophones and array length could
 365 improve array performance.

366

REFERENCES

- 367 [1] R. Karsten, A. Swan, and J. Culina, "Assessment of arrays of in-stream tidal turbines in the Bay of Fundy," *Phil. Trans. R. Soc. A*,
 368 vol. 371, no. 1985, p. 20120189, 2013.
- 369 [2] R. Inger, M. J. Attrill, S. Bearhop, A. C. Broderick, W. James Grecian, D. J. Hodgson, C. Mills, E. Sheehan, S. C. Votier, M. J. Witt
 370 *et al.*, "Marine renewable energy: potential benefits to biodiversity? An urgent call for research," *Journal of Applied Ecology*, vol. 46,
 371 no. 6, pp. 1145–1153, 2009.
- 372 [3] M. J. Dadswell, "Occurrence and migration of fishes in Minas Passage and their potential for tidal turbine interaction," 2010.
- 373 [4] A. Redden and M. Stokesbury, "Acoustic tracking of fish movements in the Minas Passage and FORCE demonstration area: Pre-turbine
 374 baseline studies (2011-2013)."
- 375 [5] D. Wang, M. Atlar, and R. Sampson, "An experimental investigation on cavitation, noise, and slipstream characteristics of ocean stream
 376 turbines," *Proceedings of the Institution of Mechanical Engineers, Part A: Journal of Power and Energy*, vol. 221, no. 2, pp. 219–231,
 377 2007.
- 378 [6] A. Lombardi, "Soundscape characterization in Grand Passage, Nova Scotia, a planned in-stream tidal energy site," 2016.
- 379 [7] M. K. Pine, A. G. Jeffs, and C. A. Radford, "Turbine sound may influence the metamorphosis behaviour of estuarine crab megalopae,"
 380 *PLoS One*, vol. 7, no. 12, p. e51790, 2012.
- 381 [8] M. Halvorsen, T. Carlson, and A. Copping, "Effects of tidal turbine noise on fish," *PNNL Report-20787 for US Dept of Energy*, WA,
 382 DC: by Pacific Northwest National Laboratory, Sequim, WA, pp. 1–41, 2011.
- 383 [9] M. Lighthill, "The Bakerian lecture, 1961. Sound generated aerodynamically," in *Proceedings of the Royal Society of London A:
 384 Mathematical, Physical and Engineering Sciences*, vol. 267, no. 1329. The Royal Society, 1962, pp. 147–182.
- 385 [10] M. Strasberg, "Nonacoustic noise interference in measurements of infrasonic ambient noise," *The Journal of the Acoustical Society of
 386 America*, vol. 66, no. 5, pp. 1487–1493, 1979.
- 387 [11] M. Van Dyke, *An album of fluid motion*. Parabolic Press Stanford, 1982, vol. 176.
- 388 [12] V. O. Knudsen, R. Alford, and J. Emling, "Underwater ambient noise," *J. Mar. Res.*, vol. 7, pp. 410–429, 1948.
- 389 [13] C. Bassett, J. Thomson, P. H. Dahl, and B. Polagye, "Flow-noise and turbulence in two tidal channels," *The Journal of the Acoustical
 390 Society of America*, vol. 135, no. 4, pp. 1764–1774, 2014.
- 391 [14] D. R. Barclay and M. J. Buckingham, "Depth dependence of wind-driven, broadband ambient noise in the Philippine Sea," *The Journal
 392 of the Acoustical Society of America*, vol. 133, no. 1, pp. 62–71, 2013.
- 393 [15] F. Dupont, C. G. Hannah, and D. Greenberg, "Modelling the sea level of the upper Bay of Fundy," *Atmosphere-Ocean*, vol. 43, no. 1,
 394 pp. 33–47, 2005.
- 395 [16] B. Wilson, R. S. Batty, and L. M. Dill, "Pacific and atlantic herring produce burst pulse sounds," *Proceedings of the Royal Society of
 396 London B: Biological Sciences*, vol. 271, no. Suppl 3, pp. S95–S97, 2004.
- 397 [17] J. A. Hildebrand, "Anthropogenic and natural sources of ambient noise in the ocean," *Marine Ecology Progress Series*, vol. 395, pp.
 398 5–20, 2009.
- 399 [18] N. D. Merchant, T. R. Barton, P. M. Thompson, E. Pirotta, D. T. Dakin, and J. Dorocicz, "Spectral probability density as a tool for
 400 ambient noise analysis," *The Journal of the Acoustical Society of America*, vol. 133, no. 4, pp. EL262–EL267, 2013.

- 401 [19] M. J. Buckingham, "On the two-point cross-correlation function of anisotropic, spatially homogeneous ambient noise in the ocean and
402 its relationship to the Green's function," *The Journal of the Acoustical Society of America*, vol. 129, no. 6, pp. 3562–3576, 2011.
- 403 [20] B. F. Cron and C. H. Sherman, "Spatial-correlation functions for various noise models," *The Journal of the Acoustical Society of*
404 *America*, vol. 34, no. 11, pp. 1732–1736, 1962.
- 405 [21] G. B. Deane, M. J. Buckingham, and C. T. Tindle, "Vertical coherence of ambient noise in shallow water overlying a fluid seabed,"
406 *The Journal of the Acoustical Society of America*, vol. 102, no. 6, pp. 3413–3424, 1997.
- 407 [22] H. Cox, "Line array performance when the signal coherence is spatially dependent," *The Journal of the Acoustical Society of America*,
408 vol. 54, no. 6, pp. 1743–1746, 1973.

409 **Matthew Auvinen** Biography text here.

PLACE
PHOTO
HERE

410

411 **David Barclay** Biography text here.

PLACE
PHOTO
HERE

412